PERGAMON

International Journal of Heat and Mass Transfer 42 (1999) 1501–1512

International Journal of HEAT and MASS TRANSFER

Moisture transport in intensive microwave heating of biomaterials: a multiphase porous media model

H. Ni[a], A.K. Datta[a,*], K.E. Torrance[b]

[a] *Department of Agricultural and Biological Engineering*, [b] *School of Mechanical and Aerospace Engineering*, *Cornell University*, *Ithaca*, *NY 14853-5701*, *U.S.A.*

Received 13 May 1997; in final form 18 March 1998

Abstract

A multiphase porous media model was developed to predict moisture transport during intensive microwave heating of biomaterials. Internal pressure gradients arise from internal heating and vaporization and significantly enhance the transport. Even a moderate internal pressure gradient in a low moisture material can cause more moisture to move to the surface than can be removed from the surface, leading to a soggy surface. A strong internal pressure gradient in a high moisture material can fully saturate the surface, leading to a very high moisture loss by liquid outflow at the surface. Addition of hot air and/or infrared heating of the surface to increase evaporation is suggested as a way to reduce surface moisture build-up.

Nomenclature

c_p specific heat [J kg^{-1} K]
c mass concentration [kg m^{-3} total volume]
C molar density of gas mixture [kmol m^{-3}]
$D_{eff,g}$ effective gas diffusivity in moist materials [m^2 s^{-1}]
D_T temperature dependence capillary diffusivity [kg m^{-1} s^{-1} K^{-1}]
D_w capillary diffusivity [m^2 s^{-1}]
F microwave flux [W m^{-2}]
h enthalpy [J kg^{-1}]; heat transfer coefficient [W m^{-2} K]
h_{mv} vapor transfer coefficient [m s^{-1}]
$\dot{I}$ volumetric evaporation term [kg m^{-3} s^{-1}]
k thermal conductivity [W m^{-1} K]; total permeability [m^2]
k_{wi}, k_{gi} intrinsic permeability at very wet stage and at very dry stage, respectively [m^2]
k_{gr}, k_{wr} gas and liquid relative permeability, respectively
K_0 $=(M_a M_v D_{eff,g})/RT[(P-p_v)M_a+p_v M_v]$
K_1–K_{18} coefficients in differential equations
m mass in representative elementary volume [kg]
M molecular weight [kg kmol^{-1}]; moisture content (dry basis or db)
$\mathbf{n}$ total flux [kg m^{-1} s]
$p_s(T)$ saturation vapor pressure of water at temperature T
p_c, p_s capillary force and saturated pressure of pure water, respectively [Pa]
P, p total pressure and partial pressure, respectively [Pa]
$\dot{q}$ volumetric heat source term [W m^{-3}]
R universal gas constant [J kmol^{-1} K]
S saturation
T temperature [K]
V volume [m^3]
x molar fraction; distance.

Greek symbols
δ penetration depth of microwave power [m]
λ latent heat of vaporization
μ dynamic viscosity [Pa s]
ρ intrinsic density [kg m^{-3}]
ρ_d density of solids in porous media [kg m^{-3} total volume]
ϕ porosity.

Subscripts
a air
amb ambient
eff effective
g gas

* Corresponding author

0017–9310/98/$ - see front matter
PII: S0017–9310(98)00123–9

ir irreducible water
s solid matrix; surface
s^- approach the surface from the inside
s^+ approach the surface from the outside
v vapor
w water
wev liquid evaporation on the surface
wp liquid 'pumping' on the surface.

1. Introduction

Microwave heating of moist biomaterials produces internal moisture distributions that are fundamentally different from those resulting from surface convective heating. An important application area is to food products that allow rapid heating in domestic microwave ovens. Moisture redistribution and loss during heating often determine the success of such food products. For example, a very moist vegetable tissue can lose too much moisture during heating, or a fried food, with a low moisture crust and a high moisture interior, can become soggy. During microwave heating, a strong filtrational flow may also arise due to internal pressures generated by vaporization [1, 2]. The present paper examines moisture transport during intensive microwave heating.

Studies on the electromagnetics and heat transfer in microwave heating [3–6] involve solutions of Maxwell's equations, either by themselves or coupled with the thermal energy equation. When coupled with the energy equation, most of the studies are for plane waves [7], which are not representative of the standing wave patterns inside a microwave cavity. Emphasis has often been on geometric effects, such as microwave reflection from multiple material surfaces or focusing due to curved surfaces. None of the foregoing studies included moisture transport. Under certain circumstances, the electromagnetic absorption can be represented as an exponential drop of energy with distance (called Lambert's absorption law). Ayappa et al. [7] developed a criterion (see also [8]) for using Lambert's law for a slab as a function of its thickness and properties, considering plane waves, but it does not apply for microwave heating in an oven. By solving Maxwell's equations in 3-D inside an oven, Peyre et al. [6] showed that for a cavity where standing wave patterns are present, the internal heating rate in a reasonably lossy material (i.e., microwave absorbing) drops approximately exponentially with distance from the surface. Such an exponential decay with distance has been used by other researchers [13] and is representative of many microwave heating applications.

Moisture transport during microwave heating can be described by multiphase porous media models of the types developed by Luikov [9] or Whitaker [10]. The model of Luikov [9] is essentially phenomenologically-based, and has been used to examine the relative effects of the phenomenological coefficients that appear. However, these coefficients are difficult to measure and interpret physically, and little data are available. In contrast with this model, the mechanistic approach (e.g., Whitaker [10]) consists of conservation equations for mass and energy for each phase (solid, liquid, and gas) with flux equations for diffusion, capillarity and Darcy flow. The transport coefficients and assumptions are better understood, and parameters are well defined and measurable. Whitaker showed that the macroscopic equations can be derived by the volume averaging of processes at the microscopic level. The literature on convective heating and drying of food, reviewed in [11] and [12], generally does not consider such comprehensive multiphase porous media models, and instead often lumps the multiphase transport processes into effective diffusivities. Such diffusivities are inappropriate for microwave heating where pressure driven flow due to internal evaporation can be a dominant effect.

Mechanistic models for the coupled heat and mass transfer during microwave heating have been developed [13–20]. When the models included microwave heating [13, 18–20] they were generally in the context of drying, which is a low power process. Heating of moist materials in a domestic microwave oven is often quite intensive. Even the study of Constant [18], which considers somewhat higher power, does not cover heating rates as high as what would be expected in a domestic microwave oven. Also, unlike drying, the materials of present interest are often very wet. Such wet materials are quite impermeable. The combination of high heating rates and low permeability is likely to generate high internal pressures, depending on the heating rates and material structure. High pressures are likely to cause strong filtrational flows which have not been studied. The pressure magnitudes are also important for material integrity and safety, as the blowing up of foods during microwave heating is well known.

At high pressures and high water contents, liquid water can directly escape across the outer boundary of a porous material, without evaporating. Previous researchers, with the exception of Constant et al. [18], have not employed this liquid outflow boundary condition. Such a boundary condition may describe the rapid moisture loss that is observed for very wet materials. In an hygroscopic material, as water is lost, the porous structure also changes (e.g., porosity increases) and therefore properties such as permeability can vary during the heating process. This effect has not been studied. Also, the strong variation of properties with moisture content, such as the capillary diffusivity, has generally been ignored. Further, in an hygroscopic material, the water is bound to the solid phase. As a result, a simple Clapeyron equation for the liquid phase does not apply. In the present study, we use experimental data on a specific material to obtain the vapor pressure as a function of saturation and temperature.

The present work considers wet, hygroscopic materials under intensive microwave heating. A transient one-dimensional formulation is used, with transport properties that can change with structure, moisture, and temperature. The specific objective are to: (1) formulate the governing equations and boundary conditions for multiphase moisture transport; (2) solve the coupled equations numerically; (3) compare the numerical results with convective (non-microwave) heating studies reported in the literature and with experimental measurements (microwave heating) of moisture loss obtained in this study; (4) compare the moisture distribution and the total moisture loss for the two extremes of high and low moisture materials; (5) assess the contribution of the convection terms to the energy equation.

2. Porous media model

2.1. Major assumptions

There are six major assumptions used in this work. (1) Each of the three phases of solid, liquid, and gas is continuous. (2) Local thermal equilibrium is valid, which means that the temperature in all three phases is equal [10]; this has been used widely in convective heating of porous media [14–17], as well as for microwave heating [13, 18–20]. (3) Biomaterials have strong physico-chemical forces between the liquid and solid matrix [21], and a vapor formula obtained from regression of experimental data is used [22]. (4) Liquid movement results from convective flow due to the gradient in total gas pressure and from capillary flow due to the gradient of capillary force, which is a strong function of moisture content. (5) The contribution of convection to energy transport is initially ignored to simplify the solution procedure, but is later added back. (6) As biomaterials lose water, the material shrinks and the gas porosity increases. However, the equivalent porosity (defined in the next section) will decrease because the total volume decreases due to shrinkage, while the volume taken by the solid matrix remains constant. Due to a lack of data on the equivalent porosity vs. moisture content, two different equivalent porosity values are used to represent high and low moisture materials.

2.2. Equilibrium state variables

In non-hygroscopic porous media, the phases of liquid, gas, and solid matrix are clearly separated. As a result, the porosity ϕ is defined as the volume fraction occupied by liquid and gas, and the liquid concentration is equal to porosity multiplied by liquid saturation. However, biomaterials can be hygroscopic, with the liquid phase bound to the solid matrix. In order to formulate equations for hygroscopic porous media analogous to those equations well-established for non-hygroscopic porous media, an equivalent porosity and equivalent water saturation are introduced.

$$\Delta V = \Delta V_s + \Delta V_w + \Delta V_g. \tag{1}$$

Equivalent porosity is defined as

$$\phi = \frac{\Delta V_w + \Delta V_g}{\Delta V}. \tag{2}$$

Equivalent saturation of liquid and gas is then defined as

$$S_w = \frac{\Delta V_w}{\Delta V_w + \Delta V_g} = \frac{\Delta V_w}{\phi \Delta V} \tag{3}$$

$$S_g = \frac{\Delta V_g}{\Delta V_w + \Delta V_g} = \frac{\Delta V_g}{\phi \Delta V}. \tag{4}$$

The mass densities of vapor, air, and their mixture are given by

$$\rho_v = \frac{\Delta m_v}{\Delta V_g} = \frac{p_v M_v}{RT} \tag{5}$$

$$\rho_a = \frac{\Delta m_a}{\Delta V_g} = \frac{p_a M_a}{RT} \tag{6}$$

$$\rho_g = \frac{\Delta m_v + \Delta m_a}{\Delta V_g} = \rho_v + \rho_a. \tag{7}$$

The mass concentrations of vapor and air are given by

$$c_v = \frac{\Delta m_v}{\Delta V} = \frac{p_c M_v S_g \phi}{RT} \tag{8}$$

$$c_a = \frac{\Delta m_a}{\Delta V} = \frac{p_a M_a S_g \phi}{RT}. \tag{9}$$

Similarly, the liquid mass concentration is given by

$$c_w = \frac{\Delta m_w}{\Delta V} = \frac{\rho_w \Delta V_w}{\Delta V} = \rho_w \phi S_w. \tag{10}$$

For the gas mixture of air and vapor, Dalton's law states that the total pressure is equal to the sum of the partial pressures of vapor and air.

$$P = p_v + p_a. \tag{11}$$

2.3. Rate laws

The total flux of vapor, $\mathbf{n}_v$, and that of air, $\mathbf{n}_a$, are composed of convective (Darcy) flow [23] and diffusion [24], respectively:

$$\mathbf{n}_v = -\rho_v \frac{k_g}{\mu_g} \nabla P - \frac{C_g^2}{\rho_g} M_a M_v D_{\mathrm{eff},g} \nabla x_v \tag{12}$$

$$\mathbf{n}_a = -\rho_a \frac{k_g}{\mu_g} \nabla P - \frac{C_g^2}{\rho_g} M_a M_v D_{\mathrm{eff},g} \nabla x_a. \tag{13}$$

The total liquid flux is composed of Darcy flow that can be further expanded in terms of total pressure and capillary pressure:

$$\mathbf{n}_w = -\rho_w \frac{k_w}{\mu_w} \nabla p_w = -\rho_w \frac{k_w}{\mu_w} \nabla (P - p_c)$$

$$= -\rho_w \frac{k_w}{\mu_w}\nabla P - D_w \rho_w \phi \nabla S_w - D_T \nabla T \quad (14)$$

where the capillary pressure p_c is a function of S_w and T, and gravitational effects are ignored. Therefore, the coefficients D_w and D_T are equal to

$$D_w = -\frac{k_w}{\phi \mu_w}\frac{\partial p_c}{\partial S_w} \quad (15)$$

$$D_T = -\rho_w \frac{k_w}{\mu_w}\frac{\partial p_c}{\partial T}. \quad (16)$$

2.4. Governing equations for mass and energy conservation

A schematic diagram of the model (1-D slab) is shown in Fig. 1. The microwaves are assumed to arrive at the left side (open boundary), where a flow of heat and moisture from the porous medium is convected away. The right side (closed boundary) is insulated and the heat and moisture fluxes are zero. On the open boundary, a diffusional flux as well as a convective flux (liquid 'pumping'), from the interior can occur. The conservation equations for vapor, liquid water, air, and energy in the porous medium are written, respectively, as

$$\frac{\partial c_v}{\partial t} + \nabla\cdot(\mathbf{n}_v) = \dot{I} \quad (17)$$

$$\frac{\partial c_w}{\partial t} + \nabla\cdot(\mathbf{n}_w) = -\dot{I} \quad (18)$$

$$\frac{\partial c_a}{\partial t} + \nabla\cdot(\mathbf{n}_a) = 0 \quad (19)$$

$$\frac{\partial}{\partial t}(c_v h_v + c_a h_a + c_w h_w + c_s h_s) + \nabla\cdot(\mathbf{n}_v h_v + \mathbf{n}_a h_a + \mathbf{n}_w h_w) = \nabla\cdot(k_{eff}\nabla T) - \lambda\dot{I} + \dot{q}. \quad (20)$$

By adding equation (17) for vapor and equation (18) for liquid, the evaporation term $\dot{I}$ can be eliminated.

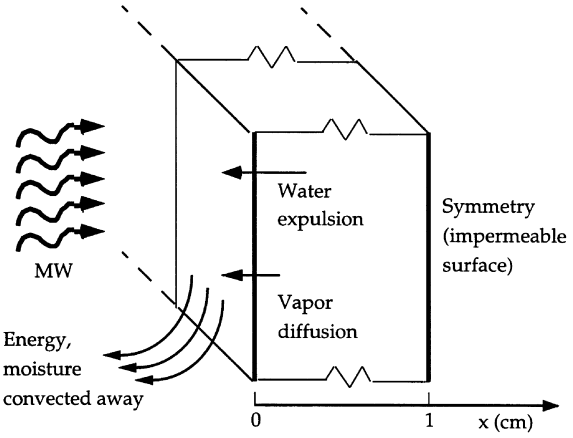

Fig. 1. Schematic diagram of the heating process with the boundary conditions.

Substituting equations (8), (10), (12) and (14), a combined equation for vapor and liquid water can be written as [25]

$$K_4\frac{\partial S_w}{\partial t} + K_5\frac{\partial T}{\partial t} + K_6\frac{\partial P}{\partial t} = \nabla\cdot(K_1\nabla S_w) + \nabla\cdot(K_2\nabla T) + \nabla\cdot(K_3\nabla P) \quad (21)$$

where the coefficient K values are described in the Appendix. For further details of equation (21) and other derivations below, the reader is referred to [25]. Similarly, after substituting equation (9) and (13), equation (19) becomes

$$K_{10}\frac{\partial S_w}{\partial t} + K_{11}\frac{\partial T}{\partial t} + K_{12}\frac{\partial P}{\partial t} = \nabla\cdot(K_7\nabla S_w) + \nabla\cdot(K_8\nabla T) + \nabla\cdot(K_9\nabla P). \quad (22)$$

The energy equation, equation (20) can be simplified as

$$(\rho c_p)_{eff}\frac{\partial T}{\partial t} + (c_{pv}\mathbf{n}_v + c_{pa}\mathbf{n}_a + c_{pw}\mathbf{n}_w)\cdot\nabla T = \nabla\cdot(k_{eff}\nabla T) - \lambda\dot{I} + \dot{q} \quad (23)$$

where

$$(\rho c_p)_{eff} = \phi(S_g\rho_g c_{pg} + S_w\rho_w c_{pw}) + (1-\phi)\rho_s c_{ps} \quad (24)$$

$$k_{eff} = \phi(S_g k_g + S_w k_w) + (1-\phi)k_s. \quad (25)$$

Ignoring the convection terms, and substituting equation (18) to replace the evaporation term $\dot{I}$, equation (23) becomes

$$K_{16}\frac{\partial S_w}{\partial t} + K_{17}\frac{\partial T}{\partial t} + K_{18}\frac{\partial P}{\partial t} = \dot{q} + \nabla\cdot(K_{13}\nabla S_w) + \nabla\cdot(K_{14}\nabla T) + \nabla\cdot(K_{15}\nabla P). \quad (26)$$

The convection term in equation (22) is ignored in all computations reported here, except in Section 4.3 where this term is added, and its contribution discussed. Therefore, equations (21), (22) and (26) form the complete equations in this system with variables S_w, T, and P. The equations are similar, thus expediting the development of a numerical code, and are applied here in transient, one-dimensional form.

2.5. Initial and boundary conditions

The initial conditions are given by uniform initial temperature T_i, uniform total pressure equal to ambient pressure P_{amb}, and uniform liquid saturation equal to S_{w_i}. The boundary conditions are:

2.5.1. Closed boundary

Boundary conditions at the closed boundary (symmetry line) and the open boundary (surface) can be significantly different. At the symmetry line, no heat or mass exchange takes place:

$$-K_1\frac{\partial S_w}{\partial x} - K_2\frac{\partial T}{\partial x} - K_3\frac{\partial P}{\partial x} = n_w + n_v = 0$$

$$-K_7\frac{\partial S_w}{\partial x}-K_8\frac{\partial T}{\partial x}-K_9\frac{\partial P}{\partial x}=n_a=0$$

$$-k_{eff}\frac{\partial T}{\partial x}=0. \quad (27)$$

2.5.2. Open boundary

At the open (left side) boundary, there is an exchange of energy, vapor, liquid, and air. Two situations can occur, depending on whether the liquid from the interior crosses the boundary with or without a complete phase change.

2.5.2.1. Open boundary without liquid 'pumping' In this case, the water flux (liquid and vapor) reaching the boundary from the interior is fully evaporated and convected away as vapor to the ambient. Regardless of the volumetric evaporation rate inside, any remaining liquid flux arriving at the surface is evaporated at the open surface. The surface evaporation is determined by the surface area covered by the liquid, and the mass and heat balances are

$$n_v+n_w|_{s^-}=n_v+n_{wev}|_{s^+}=\phi(S_g+S_w)\left(\frac{p_v}{R_vT}-\rho_{v0}\right)h_{mv}$$

$$P|_s=P_{amb}$$

$$n_vh_v+n_wh_w+n_ah_a-k_{eff}\left.\frac{\partial T}{\partial x}\right|_{s^-}$$

$$=(n_v+n_w)h_v+n_ah_a|_{s^+}+h(T-T_{amb}) \quad (28)$$

where h_{mv} and h are the vapor and convective mass and heat transfer coefficients, respectively, and h_v and h_a are the water vapor and air enthalpies, respectively. Equation (28) can be rewritten as the following, consistent with the governing equations

$$-K_1\frac{\partial S_w}{\partial x}-K_2\frac{\partial T}{\partial x}-K_3\frac{\partial P}{\partial x}=n_{wev}+n_v|_{s^+}$$

$$=\phi(S_g+S_w)\left(\frac{p_v}{R_vT}-\rho_{v0}\right)h_{mv}$$

$$P|_s=P_{amb}$$

$$-k_{eff}\frac{\partial T}{\partial x}=h(T-T_{amb})+n_{wev}\lambda|_{s^+}. \quad (29)$$

There are two ways to replace the liquid water evaporation rate, n_{wev}, in equation (29). One is to use $n_{wev}=\phi S_w[(p_v/R_vT)-\rho_{v0}]h_{mv}$ and the other is to substitute equation (14) for the liquid flux, n_w. Performing the latter substitution, equation (29) becomes

$$-K_{13}\frac{\partial S_w}{\partial x}-K_{14}\frac{\partial T}{\partial x}-K_{15}\frac{\partial P}{\partial x}=h(T-T_{amb}). \quad (30)$$

2.5.2.2. Open boundary with liquid 'pumping' When the internal pressure gradient pushes more liquid to the open boundary than can be evaporated there, the surface of the porous medium becomes fully saturated. The liquid water becomes free, and the capillary forces cannot hold the liquid within the pores; the liquid pressure at the surface becomes the same as the ambient gas pressure, which is atmospheric. Even a small pressure gradient in the liquid toward the surface can cause liquid to flow across the open boundary without phase change. We call this process 'pumping'. The pumped water is not fully evaporated at the open boundary (it can leave the surface as a liquid). The criterion for the 'pumping' is formulated as [18]

$$S_w|_s=1$$

$$\left.\frac{\partial p_w}{\partial x}\right|_s>0. \quad (31)$$

When these conditions are satisfied, the following boundary conditions are used

$$n_v+n_w|_{s^-}=n_v+n_{wev}+n_{wp}|_{s^+}$$

$$=\phi(S_g+S_w)\left(\frac{p_v}{R_vT}-\rho_{v0}\right)h_{mv}+n_{wp}|_{s^+}$$

$$P|_s=P_{amb}$$

$$n_vh_v+n_wh_w+n_ah_a-k_{eff}\left.\frac{\partial T}{\partial x}\right|_{s^-}$$

$$=n_vh_v+n_{wev}h_v+n_{wp}h_w+n_ah_a|_{s^+}+h(T-T_{amb}) \quad (32)$$

where $n_w=n_{wev}+n_{wp}$. Consistent with the final governing equations, equation (32) can be further rewritten as:

$$-K_1\frac{\partial S_w}{\partial x}-K_2\frac{\partial T}{\partial x}-K_3\frac{\partial P}{\partial x}$$

$$=n_v+n_w|_{s^+}=\phi(S_g+S_w)\left(\frac{p_v}{R_vT}-\rho_{v0}\right)h_{mv}+n_{wp}|_{s^+}$$

$$P|_s=P_{amb}$$

$$-k_{eff}\left.\frac{\partial T}{\partial x}\right|_{s^-}=\lambda n_{wev}|_{s^+}+h(T-T_{amb}). \quad (33)$$

Since the liquid is pumped out due to the total pressure gradient,

$$n_{wp}=-\rho_w\frac{kk_{wr}}{\mu_w}\frac{\partial P}{\partial x}. \quad (34)$$

Substituting equations (34) and (14), equation (33) becomes

$$-K_1\frac{\partial S_w}{\partial x}-K_2\frac{\partial T}{\partial x}-\left(K_3-\rho_w\frac{kk_{wr}}{\mu_w}\right)\frac{\partial P}{\partial x}$$

$$=\phi(S_g+S_w)\left(\frac{p_v}{R_vT}-\rho_{v0}\right)h_{mv}$$

$$P=P_{amb}$$

$$K_{13}\frac{\partial S_w}{\partial x}-K_{14}\frac{\partial T}{\partial x}=h(T-T_{amb}). \quad (35)$$

2.6. Microwave power density

For this study, a simplified electromagnetics is assumed with an exponential drop of the absorbed energy with

distance inside the porous medium, as discussed in the literature review, and as used by most microwave heating studies [18, 13, 27]. Following this, the microwave flux at a position x is given by

$$F(x) = F_s \exp\left(-\frac{x}{\delta}\right) \tag{36}$$

where F_s is the microwave flux at the surface, and δ is the penetration depth of the microwaves. The penetration depth is primarily a function of moisture content; it varies spatially and is estimated [25] from typical dielectric property data [26]. Equation (36) for the microwave flux term can be modified [28] for a varying penetration depth as

$$F(x) = F_s \exp\left(-\int_0^x \frac{dx}{\delta(x)}\right). \tag{37}$$

The volumetric heat source term in the governing energy equation can be deduced from the flux equation given by equation (37) as

$$\dot{q}(x) = \frac{dF}{dx} = \frac{F_s}{\delta(x)} \exp\left(-\int_0^x \frac{dx}{\delta}\right). \tag{38}$$

Equation (38) provides a simplified estimate for the microwave volumetric heating for many applications, and allows us to focus on the mass and heat transfer processes.

2.7. Input parameters

Some of the input data are given in Table 1. A sample thickness of $x = 1$ cm will be considered, with initial liquid saturations of $S_w = 0.5$ and 0.8. The corresponding initial microwave penetration depths are $\delta = 4.6$ and 0.9 cm, respectively. Further details, except for the vapor pressure and permeability data, are discussed in [25]. A sensitivity study is also contained in [25] which helped identify appropriate parameters. The vapor pressure (p_v) was considered as a function of both temperature and saturation of the material. This relationship was available for potato material from the work of Ratti et al. [22] as below:

$$\ln\frac{p_v}{p_s(T)} = -0.0267M^{-1.656} + 0.0107e^{-1.287M}M^{1.513}\ln p_s(T) \tag{39}$$

where $p_s(T)$ and M are the vapor pressure of pure water at temperature T and the moisture content of the material, respectively.

The temperature coefficient of capillarity (D_T) is ignored in this study. The permeability can be represented as the product of intrinsic permeability and relative permeability [23]. The intrinsic permeability does not vary with moisture content for non-hygroscopic materials since the structure of the solid phase remains fixed. However, for biomaterials (hygroscopic), the intrinsic permeability increases as moisture decreases due to the development of additional gas pore spaces. Shrinkage further modifies this relationship. An approximate procedure to consider the effect of structural change on permeability is now described.

Intrinsic permeability in the very wet stage and the very dry stage are not the same. The total permeability for gas (k_g) and water (k_w) is calculated by using two different intrinsic permeabilities k_{gi} and k_{wi} for gas and water, respectively, as

$$k_g = k_{gi}k_{gr}$$
$$k_w = k_{wi}k_{wr} \tag{40}$$

where the relative permeabilities k_{gr} and k_{wr} are given by [23]

$$k_{gr} = 1 - 1.1S_w \quad S_w < 1/1.1$$
$$k_{gr} = 0 \quad S_w > 1/1.1$$
$$k_{wr} = \left(\frac{S_w - S_{ir}}{1 - S_{ir}}\right)^3 \quad S_w > S_{ir} \tag{41}$$

Table 1
Some of the input parameters used in the computations

Input parameter	Low-moisture material	High-moisture material
Porosity, ϕ	0.75	0.88
Initial saturation, S_w	0.5	0.8
Irreducible saturation, S_{ir}	0.09	0.09
Intrinsic permeability at very dry state, k_{gi} ($\times 10^{-14}$ m^2)	10	10
Intrinsic permeability at very wet state, k_{wi} ($\times 10^{-14}$ m^2)	5	5
Surrounding temperature, T_a (°C)	20	20
Surrounding vapor density, ρ_v (kg m^{-3})	0	0
Heat transfer coefficient, h (W m^{-2} K^{-1})	20	20
Mass transfer coefficient, h_{mv} (m s^{-1})	0.01	0.01
Microwave surface flux, F_0 (W m^{-2})	30 000	30 000

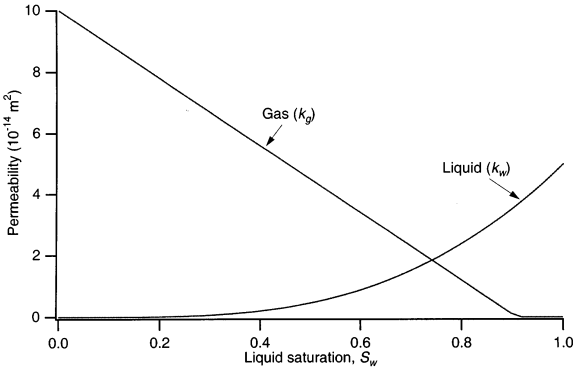

Fig. 2. Permeabilities k_w and k_g, calculated from intrinsic and relative permeabilities, plotted vs. saturation.

$$k_{wr} = 0 \quad S_w < S_{ir} \tag{42}$$

and S_{ir} is the irreducible liquid saturation. Equations (40)–(42) are shown graphed in Fig. 2, using the k_{gi}, k_{wi}, and S_{ir} values from Table 1. At high water content, the total gas permeability decays linearly to zero. The total liquid permeability is high at high liquid saturation, but not as large as the total gas permeability at very low liquid saturation. This is the effect of the change in structure (more gas pores). In reality, the intrinsic permeability changes continuously from the very wet stage to the very dry stage. In the absence of such data, the curves in Fig. 2 are a reasonable description of the effect of structural changes on permeability.

2.8. Numerical scheme and the solution procedure

A finite difference method is used with central space differencing for the diffusion terms, Crank–Nicolson time differencing, and upwind differencing of the convection terms when they are included. All equations are assembled in one matrix and are solved simultaneously using the LAPACK library on an IBM SP2 supercomputer. A uniform grid system is used with 41 nodes over a total material thickness of 1 cm. For the convective heat and mass transfer term on the open boundary, the values at the previous time step are used for simplicity. Although there is a time lag, the error is small because the rate of boundary value changes is small. The heat source term is evaluated with values from the previous time step—this kept the computations stable. A rather small time step is used. Iteration over a time step is employed to handle non-linearities, and is continued until two consecutive iterations produce results within a certain tolerance.

Convergence of the numerical results was verified through mesh convergence, going up to 101 nodes in the 1 cm thickness. Energy and mass conservation of the numerical model was also checked at different times during heating. The cumulative heat loss from the surface was compared with the aggregate of sensible heat, latent heat from evaporation, and the microwave heat source. Likewise, the moisture loss from the surface was compared with the decrease in liquid water inside. The relative error increased with heating time but the largest value of the relative error after 90 s of heating was 2.6×10^{-3}%. Although the inside pressure rises due to internal evaporation and gases are expelled at an increasing velocity, it was verified that sonic choking in the porous medium did not arise. Further details of the numerical methods, including the finite difference equations, are available in [25].

3. Model validation

3.1. Comparison with other numerical predictions

To check the accuracy, calculations from the present model were compared with previous numerical predictions for convective drying of clay brick [15]. Details of the input parameters are given in [25]. Comparison of temperature values in Fig. 3 (upper graph) shows the same trend, although the wet bulb temperature in our

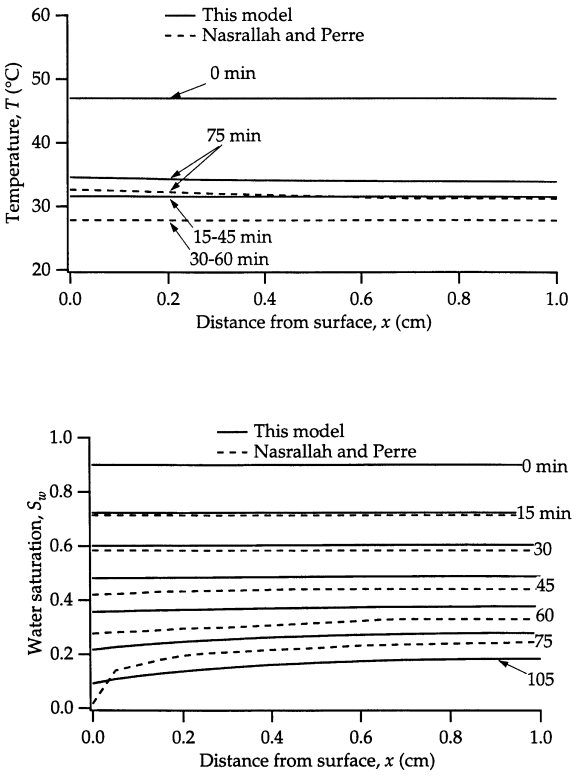

Fig. 3. Comparison of temperature and water saturation with those of Nasrallah and Perre.

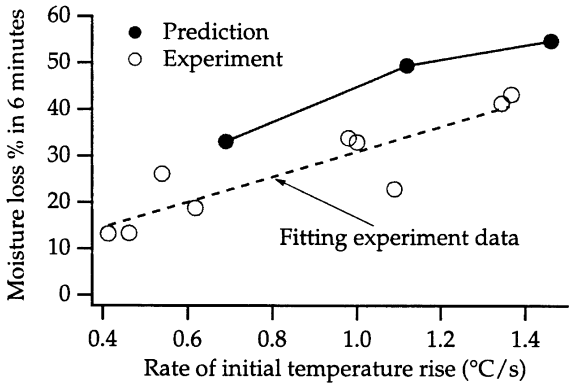

Fig. 4. Comparison of experimental data and model prediction of moisture loss in a high moisture material after 6 min of heating.

prediction was about 4°C lower than in [15]. Comparison of water saturation in Fig. 3 (lower graph) also shows similar trends, although the spatial variation of water saturation near the surface predicted by our model is more gradual. This might be due to an insufficient mesh near the surface for the uniform grid we used.

3.2. Comparison with experiments

The heating rate (i.e., the initial rate of temperature rise) and total moisture loss were measured for a high moisture material (raw potatoes). To emulate a 1-D system, the sides of the samples were covered with a reflective foil to prevent microwave penetration. The measured heating rate is used, as opposed to the microwave oven power level, since the heating rate is a complex function of oven power [25]. Inside the oven, a fiberoptic temperature probe (Photonetics, Inc., Wakefield, MA) was used that does not interfere with the microwaves. The temperature–time curves follow a fairly straight line until about 80°C. This temperature region was used to calculate the heating rate (the slope of the temperature–time curve). The measured moisture loss vs. heating rate is shown in Fig. 4, and follows the same trend as the model predictions. Considering the difficulties in the experimentation, the comparison shown is regarded as satisfactory.

4. Results and discussion

The results are divided into two parts that cover, on the one extreme, a low moisture material (moisture content of 1.06 on a dry basis or d.b.) that has a high gas permeability, and a low liquid permeability, so that the transport is mostly in the vapor phase and the pressures developed are lower. The other extreme is a high moisture material (4.2 d.b.) that has a low gas permeability, and a high liquid permeability. The higher moisture, however, leads to much higher microwave absorption (faster heating). Faster heating, combined with the lower hydraulic conductivity of water, leads to the development of much higher internal pressures. The calculated results reveal that the high moisture situation is prone to liquid being 'pumped' out at the surface. For both low and high moisture materials (Figs 5 and 6), the symmetry boundary condition given by equation (27) leads to flat profiles for temperature, moisture, and pressure near the symmetry line ($x = 1$ cm).

4.1. Low-moisture material

Temperature profiles for the microwave heating of a low moisture material are shown in Fig. 5a. The temperature increase with time is fairly slow since the rate of microwave absorption is lower at this low moisture content, and the surface temperature stays colder due to the cold surrounding air. The moisture profiles are shown in Fig. 5b. In the first six minutes the moisture level near the surface drops in a manner similar to convective surface heating. In such an application, the lower internal temperatures cause a lower rate of evaporation and lower pressure generation than for microwave heating; therefore, there is insignificant pressure driven flow.

With microwave heating, as temperatures inside rise closer to 100°C, evaporation increases and the internal pressure starts to build. Even small amounts of pressure can cause enough moisture to reach the surface, exceeding its moisture removal capacity, and causing moisture accumulation near the surface. Thus, the first signs of moisture accumulation, at about seven minutes (Fig. 5b), correspond to an excess pressure of only about 2 kPa (0.02 atm) in the interior. Hence, even a small pressure differential can lead to a soggy surface. Total pressure profiles for the microwave heating process are shown in Fig. 5c. Interior pressures increase monotonically with time over the time interval shown, and in space, with the maximum interior values occurring at the symmetry plane.

With time, the surface moisture increases and, after about eight minutes, the surface is much wetter than it was initially. Continued microwave heating would eventually cause the surface moisture level to drop since the moisture level inside the material would decrease and lead to decreased microwave absorption, reduced evaporation, and pressure generation. The observed moisture saturation profiles are fundamentally different from those due to capillary diffusion alone, as in the case of surface convection heating, where the moisture moves down a moisture gradient from regions of high moisture to low moisture.

The average moisture content and rate of moisture loss during heating are shown in Fig. 5d. The rate of total

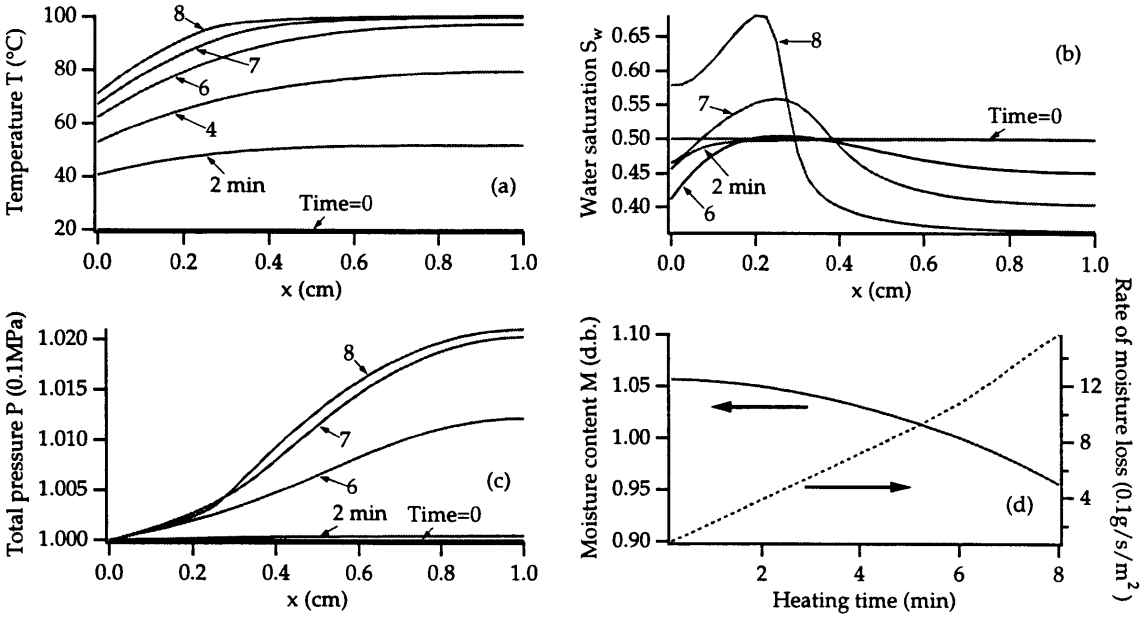

Fig. 5. General profiles during microwave heating of a low moisture material: input data from Table 1.

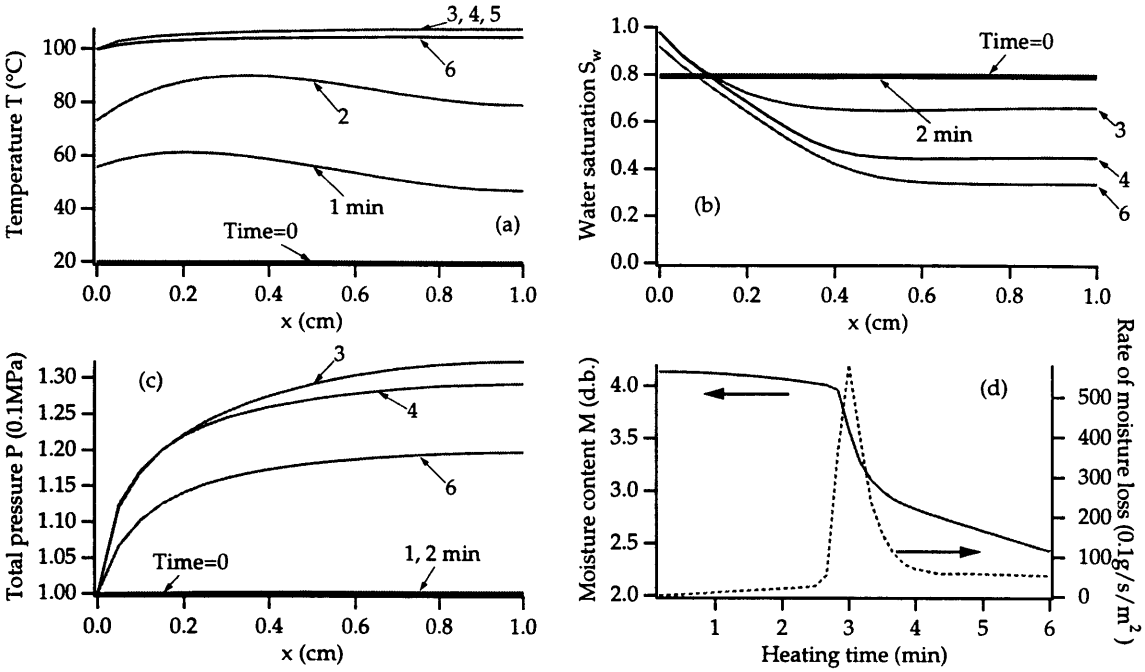

Fig. 6. General profiles during microwave heating of a high moisture material. Increased moisture loss after 3 min is due to a 'pumping effect' whereby liquid water leaves the boundary without being evaporated: input data from Table 1.

moisture loss keeps increasing until 8 min as the surface gets hotter and wetter, increasing the vapor pressure at the surface. For longer heating times, the rate of moisture loss decreases.

4.2. High-moisture material

Food materials such as raw vegetables are considered representative of materials with a very high initial moisture content. If the microwave power is low (drying), the temperature, moisture, and pressure profiles are similar to those of the low moisture material discussed in the previous section. At high power (heating), the profiles are expected to be much different because a liquid pumping condition can occur at the surface.

Temperature profiles for a high moisture material are shown in Fig. 6a. The internal temperature quickly reaches the boiling point (in about three minutes) and a maximum temperature of 107°C occurs. The heating rate used is 0.69°C/s, which is higher than that used for the low moisture material (0.27°C/s). After about three minutes, the temperature in Fig. 6a starts to drop because the moisture inside becomes lower, decreasing the microwave absorption and, therefore, the evaporation rate and pressure development. The temperature on the surface is always lower than in the interior, but not as low as in the case of low moisture heating (Fig. 5a). Total pressure profiles are shown in Fig. 6c. Pressure inside reaches an overpressure of about 32 kPa (0.32 atm), which is much higher than in the case of low moisture heating (Fig. 5c). Rapid development of this high pressure fundamentally changes the moisture profiles, as discussed below. The pressure eventually drops as moisture is depleted.

Water saturation profiles for the high-moisture material are shown in Fig. 6b. In the very initial stages (the first minute) of heating, the moisture level drops near the surface in a manner similar to convective heating. However, at about three minutes, the surface starts to accumulate moisture until it becomes almost fully saturated. The generated pressure (Fig. 6c) continues to push interior liquid water to the surface, until the surface cannot hold any more. The capillary force tends to zero when the material is fully saturated. After this, liquid is pumped across the open boundary without undergoing a phase change. The large drop in internal moisture after about three minutes (Fig. 6d) is due to this surface pumping phenomena. Note that the near-surface pressure gradient condition, equation (31), acts like a switch that controls the two mechanisms of moisture loss at the open boundary. The surface liquid saturation first increases to unity, and then pumping starts when the internal pressure gradient builds up. Thus, there is no discontinuity for the two types of boundary condition [equations (29) and (33)], but a simple transition from one to the other. The rate of moisture also is shown in Fig. 6d, and eventually drops but does so slowly since the temperature and moisture at the surface are still comparatively high.

4.3. Contribution of convection to energy transport

As stated in the assumptions, the convection terms in the thermal energy equation [equation (23)] have been ignored to simplify the solution. To justify this assumption, the convection terms were added back to the energy equation.

Profiles with the convection terms present for a low moisture material are shown in Fig. 7. These results can be compared with Fig. 5. For a low moisture material, since there is a large spatial temperature variation (and spatial gradient), the convection terms in the energy equation bring more energy from the inside to the surface so that the surface temperature is a little higher. Consequently, the internal moisture is pushed toward the surface so that there is a sharper moisture interface inside (at about $x = 0.2$ cm). The surface water saturation is also somewhat higher. Qualitatively, however, the profiles in the interior are the same as those without the convection terms. A similar, but stronger, conclusion follows for a high moisture material. In this case there is generally only a small internal temperature variation (and temperature gradient). Profiles with the convection terms included [25] essentially replicate these without the convection terms (Fig. 6). The foregoing justifies dropping the convection terms for both the low and high moisture materials of the present study.

Although not reported here, further sensitivity analyses were carried out for the heat and mass transfer model [25]. Increasing thickness of the slab did not change the profiles qualitatively. A larger liquid permeability when the material is very wet increases the internal moisture transport, leading to a wetter surface. Decreasing the gas permeability leads to much higher pressures and an increased water flux toward the surface. A higher heating rate leads to faster changes in temperature, moisture, and pressure, and increased moisture loss. In a 2-D geometry, which was also considered, microwaves arrive from two sides and the heating rates are faster, making the effect qualitatively equivalent to that due to higher heating rates in a 1-D geometry.

5. Conclusions

The following conclusions may be drawn from this study. (1) A multiphase transport model of an hygroscopic porous media was developed that includes spatially varying and intense internal heat generation, evaporation, and pressure driven flow. The transport properties varied with structure, moisture, and temperature. The model predicts the moisture movement in wet biomaterials under intensive microwave heating. (2) The

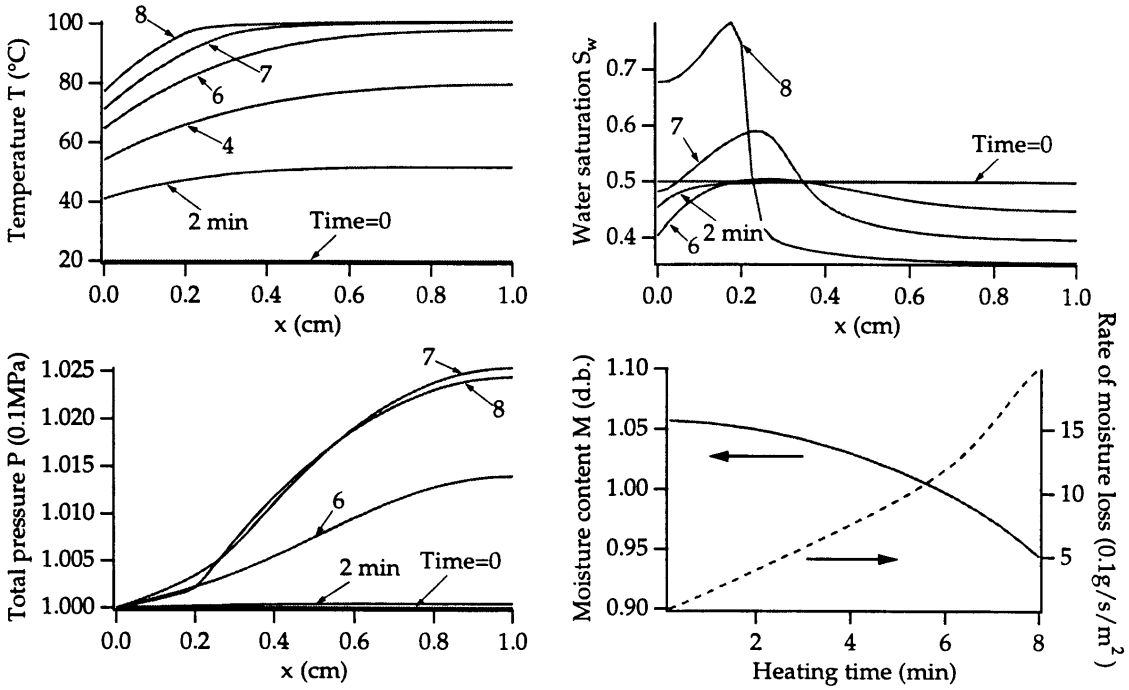

Fig. 7. General profiles during microwave heating of a low moisture material, computed with convection terms in the energy equation.

moisture level on the surface increases significantly due to the rate of transport from inside exceeding the rate of removal from the surface. This can make a dry surface soggy. (3) In a high moisture material, as compared to a low moisture material, rates of heating are higher and moisture loss is much higher, due to liquid water escaping from the surface without undergoing a change of phase. The liquid water is driven (i.e., pushed) by the higher pressures inside. Combining microwave with hot air and/or infrared heating is suggested to increase the surface temperature and remove the surface moisture build up. (4) The contribution from the convection terms in the energy equation appears to be relatively minor. Although the current study was motivated by microwave food heating, the results may be relevant to a broader class of engineering materials.

Acknowledgement

Some of the computing resources were provided by the Cornell Theory Center, which receives major funding from NSF and New York State with additional support from ARPA, the National Center for Research Resources at NIH, IBM Corporation, and members of the Corporate Research Institute.

Appendix

$$
\begin{aligned}
K_1 &= K_0 P \frac{\partial p_v}{\partial S_w} + D_w \\
K_2 &= K_0 P \frac{\partial p_v}{\partial T} + D_T \\
K_3 &= \frac{p_v M_v}{RT} \frac{kk_{gr}}{\mu_g} - K_0 p_v + \rho_w \frac{kk_{wr}}{\mu_w} \\
K_4 &= -\phi \frac{p_v M_v}{RT} + \frac{\phi(1-S_w)}{R_v T} \frac{\partial p_v}{\partial S_w} + \phi \rho_w \\
K_5 &= \frac{\phi(1-S_w) M_v}{R} \frac{\partial}{\partial T}\left(\frac{p_v}{T}\right) \\
K_6 &= 0 \\
K_7 &= -K_0 P \frac{\partial p_v}{\partial S_w} \\
K_8 &= -K_0 P \frac{\partial p_v}{\partial T}
\end{aligned}
\tag{43}
$$

$$
\begin{aligned}
K_9 &= \frac{(P-p_v) M_a}{RT} \frac{kk_{gr}}{\mu_g} + K_0 p_v \\
K_{10} &= -\frac{\phi M_a}{R}\left(\frac{P-p_v}{T} + \frac{1-S_w}{T} \frac{\partial p_v}{\partial S_w}\right) \\
K_{11} &= -\frac{\phi M_a}{R}\left\{\frac{P}{T^2} - \frac{P S_w}{T^2} + (1-S_w) \frac{\partial}{\partial t}\left(\frac{p_v}{T}\right)\right\} \\
K_{12} &= \frac{\phi(1-S_w) M_a}{RT}
\end{aligned}
\tag{44}
$$

$$K_{13} = -D_w\lambda$$
$$K_{14} = k_{eff} - D_T\lambda$$
$$K_{15} = -\frac{kk_{wr}}{\mu_w}\rho_w\lambda$$
$$K_{16} = -\lambda\phi\rho_w$$
$$K_{17} = (\rho c_p)_{eff}$$
$$K_{18} = 0. \quad (45)$$

References

[1] Lyons DW, Hatcher JD. Drying of a porous media with internal heat generation. Int J Heat and Mass Transfer 1972;15:897–905.

[2] Perkins RM. The heat and mass transfer characteristics of boiling point drying using radio frequency and microwave electromagnetic fields. Int J Heat and Mass Transfer 1980;23:687–95.

[3] Ayappa KG. Modeling transport processes during microwave heating : a review. Reviews in Chemical Engineering 1997;13(2):1–68.

[4] Fu WB, Metaxas AC. Numerical prediction of three-dimensional power density distribution in a multi-moded cavity. J Microwave Power and Electromagnetic Energy 1994;29:67–75.

[5] Jia X, Jolly P. Simulation of microwave field and power distribution in a cavity by a three-dimensional finite element method. J Microwave Power and Electromagnetic Energy 1992;27(1):11–22.

[6] Peyre F, Datta A, Seyler CE. Influence of the dielectric property on microwave oven heating patterns : applications to food materials. J Microwave Power and Electromagnetic Energy 1997;32(1):3–15.

[7] Ayappa KG, Davis HT, Crapiste G, Davis EA, Gordon J. Microwave heating : an evaluation of power formulations. Chemical Engineering Science 1991;46(4):1005–16.

[8] Fu WB, Metaxas AC. A mathematical derivation of power penetration depth for thin lossy materials. J Microwave Power and Electromagnetic Energy 1994;27:217–22.

[9] Luikov AV. Systems of differential equations of heat and mass transfer in capillary-porous bodies (review). Int J Heat and Mass Transfer 1975;18(1-A):1–13.

[10] Whitaker S. Simultaneous heat, mass and momentum transfer in porous media : a theory of drying. Adv Heat Transfer 1977;13:119–203.

[11] Bruin S, Luyben K. Drying of food materials : a review of recent developments. Adv in Drying 1980;1:155–215.

[12] Fortes M, Okos MR. Drying theories : their bases and limitations as applied to foods and grains. Adv in Drying 1980;1:119–54.

[13] Wei CK, Davis HT, Davis EA, Gordan J. Heat and mass transfer in water-laden sandstone : microwave heating. AIChE J 1985;31(5):842–8.

[14] Stanish MA, Schajer GS, Kayihan F. A mathematical model of drying for hygroscopic porous media. AIChEJ 1986;32(8):1301–11.

[15] Nasrallah SB, Perre P. Detailed study of a model of heat and mass transfer during convective drying of porous media. Int J Heat and Mass Transfer 1988;31(5):957–67.

[16] Ilic M, Turner IW. Convective drying of a consolidated slab of wet porous material. Int J Heat and Mass Transfer 1989;32(1):2351–62.

[17] Chen P, Pei D. A mathematical model of drying processes. Int J Heat and Mass Transfer 1989;32(2):297–310.

[18] Constant T, Moyne C, Perre P. Drying with internal heat generation : theoretical aspects and application to microwave heating. AIChE J 1996;42(2):359–68.

[19] Perre P, Moyne C. Processes related to drying, Part II : use of the same model to solve transfers both in saturated and unsaturated porous media. Drying Technology 1991;9(5):1153–79.

[20] Turner IW, Jolly PG. Combined microwave and convective drying of a porous material. Drying Technology 1991;9(5):1209–69.

[21] Rizvi SSH. Thermodynamic properties of foods in dehydration. In Rao. MA, Rizvi SSH. editors. Engineering properties of foods. New York : Marcel Dekker, 1995.

[22] Ratti C, Crapiste GH, Rotstein E. A new water sorption equilibrium expression for solid foods based on thermodynamic considerations. J Food Science 1989;54(3):738–47.

[23] Bear J. Dynamics of fluids in porous media. New York : American Elsevier, 1972.

[24] Bird RB, Stewart WE, Lightfoot, EN. Transport phenomena. New York : Wiley, 1960.

[25] Ni H. Multiphase moisture transport in porous media under intensive microwave heating. Ph.D. thesis, Cornell University, 1997.

[26] Metaxas AC, Meridith RJ. Industrial microwave heating. London : Peter Peregrinus Ltd, 1988.

[27] Zeng X, Faghri A. Experimental and numerical study of microwave thawing heat transfer for food materials. J Heat Transfer 1994;116:446–55.

[28] Ni H, Datta AK, Parmeswar R. Prediction of moisture loss and its relation to heating uniformity in microwaved foods. Proceedings of 29th Microwave Power Symposium, Chicago, IL, 1994.